Self-Assembled Molecules as Selective Contacts in $CsPbBr_3$ Nanocrystal Light Emitting Diodes

Sarika Kumari,[a,b] José G. Sánchez,[a] Muhammad Imran,[c] Ece Aktas,[a,†] Dora A. González,[a,d] Liberato Manna,[c] Eugenia Martínez-Ferrero,[a,b,§,*] Emilio Palomares[a,e]

Metal halide perovskite nanocrystals have demonstrated their potential as light sources when forming part of efficient light emitting diodes (LEDs). However, operational stability and efficiency are compromised primarily because of unstable hole transport layers. In this work, we report the application of two carbazole-based self-assembled molecules (SAMs) as hole injecting materials in perovskite-based LEDs. Their structures differ in one phenyl ring in the bridge; however, the extra ring provides more stability to the devices, even surpassing the one obtained with the widely used polymer PTAA. In addition, due to the structural and electronic characteristics of the SAMs, the efficiency of the devices is also increased

.

Introduction

Metal halide perovskite (MHP) semiconductors with the general formula ABX_3, where A and B are monovalent and divalent cations (A = $CH_3NH_3^+$, Cs^+, $HC(NH_2)^{2+}$, B= Pb^{2+}, Sn^{2+}) and X is the halide anion (Cl^-, Br^-, I^-), have attracted much interest since the seminal paper of Miyasaka et al.[1,2] In addition to their low-temperature synthesis and solution processability, metal halide perovskites have tunable emission wavelength, good photoluminescent quantum yield, high absorption coefficient, high charge-carrier mobility, low excitonic binding energy and long excitonic diffusion length.[3] With such physical properties, these materials have not only been assessed in solar cells but also in light-emitting diodes (LEDs),[4] photodetectors,[5,6] and LASERs.[7] In particular, the excellent properties of the light emission in metal halide perovskites, such as narrow spectral distribution and high color purity, have pushed their application in perovskite-based LEDs (PeLEDs).[8] A pioneering work in 2014 reported green light emission and external quantum efficiency (EQE) of 0.1%.[9] Since then, research has rapidly expanded and the maximum EQE achieved over the past 6 years has increased up to 23.8% for green LEDs,[10] which is comparable to CdSe-based quantum dot LEDs.[11] However, despite these promising results, PeLEDs still face several challenges to approach commercial market counterparts, which are the toxicity of the constituent elements, the long-term stability and efficiency.[12] Lead can be replaced by tin which show potential for efficient and stable solar cells.[13,14] Regarding stability and efficiency, both concepts are interrelated since PeLEDs work under high current densities and relatively high external applied bias, which increases the stress on the materials. On the one hand, the operational instability can be caused by the presence of defects and the ion migration process present in ABX_3 perovskite materials, the charge accumulation at the interfaces and the generation of local heat. On the other hand, the decrease in efficiency is also related to the presence of charge trapping induced by defects, the effect of ion mobility, weak light outcoupling efficiency and additionally by the existence of unbalanced charge injection into the active layer.

One strategy to reduce ion mobility and the presence of defects has been to prepare low-dimensional perovskites such as colloidal perovskite $CsPbBr_3$ nanocrystals (MHP NCs). These nanometer-sized semiconductors, whose size typically ranges between 2-20 nm, exhibit narrow full-width at half maximum (FWHM) photoluminescence (PL), hence high color purity, and high PL quantum yield, both features strongly required for LED application.[15] Furthermore, the density of surface defects of MHP NCs can be reduced by proper surface passivation. Yet, the presence of defects at the interface between the NCs and the carrier transport layers also affects charge transport and injection and, consequently, the stability of the device. In this direction, molecular passivation of the perovskite interfaces has demonstrated its potential to reduce non-radiative recombination and increase the stability of the devices.[16,4]

In this work, we report the application of self-assembled molecules (SAMs) as hole transport materials (HTM) to improve charge injection and the stability of the LEDs. SAMs have been previously applied in perovskite-based solar cell devices by our group[17,18] and by others[19,20]. All these works have demonstrated the ability of SAMs to improve the power conversion efficiency and increase the device stability compared to conventional organic hole transport layers. Nonetheless, their application in LEDs is scarce,[21,22] and, to the best of our knowledge, SAMs have not been applied in PeLEDs. SAMs consist of organic moieties that can be deposited onto the transparent conducting oxide

(TCO) electrode forming a nanoscale layer that modifies the surface energy, the work function, and the wettability of the inorganic substrates at the interface. Conventional hole transport materials such as poly(3,4-ethylenedioxythiophene) polystyrene sulfonate (PEDOT:PSS) have high solution processability, moderate band gap (2.9 eV), good thermal stability, high transmittance in the visible range and adequate hole conductivity. However, the hygroscopic and acidic nature of PEDOT:PSS are a cause of degradation in the devices, which reduces their lifetime.[23] PTAA, (poly [bis(4-phenyl) (2,5,6-trimethylphenyl) amine), another popular HTM, is more hydrophobic but has high cost (1000 euros/gr), that limits its potential use in large scale industrialization. Therefore, the substitution of these materials by nanoscale SAMs simplifies the device architecture, avoids interlayer mixing and lowers the cost of the materials and of the final device.

Herein, we have exploited two carbazole-based self-assembled molecules, **EADR03**, (4-(3,6-bis(2,4-dimethoxyphenyl)-9*H*-carbazol-9-yl) benzoic acid) and **EADR04**, (4'- (3,6-bis (2,4-dimethoxyphenyl) - 9*H*-carbazol-9-yl) - [1,1'-biphenyl] - 4 - carboxylic acid) (see Scheme 1a), to enhance the hole injection in $CsPbBr_3$ PeLEDs. Such devices (measured in controlled atmosphere without encapsulation) featured an increase in the luminance and lifetime compared to the devices prepared with PTAA or without HTM.

Experimental

Synthesis of $CsPbBr_3$

Cesium oleate was prepared by dissolving 81.4 mg of cesium carbonate (Cs_2CO_3, Aldrich, 99.9%) into 4 mL of octadecene (ODE, Sigma-Aldrich, 90%) and 250 µl of oleic acid (OA, Sigma Aldrich, 90%) while degassing the solution with the help of Schlenk line under a vacuum of $5{\cdot}10^{-1}$ mbar at 80 ºC for 3h with continuous stirring. Since cesium oleate precipitates out of ODE at room temperature, it was preheated to 100 ºC before injection. 345 mg of $PbBr_2$ in a three-neck flask, 25 mL of ODE, and two commonly used organic surface ligands, 2.5 mL of OA and 2.5 mL of oleylamine (OLA), were degassed in different flasks under the same conditions than cesium oleate. After degassing, ODE, OA and OLA were injected into the three-neck flask containing the lead bromide to dissolve it completely under vacuum at 120 ºC with continuous vigorous stirring. After the complete dissolution of $PbBr_2$, the flask was slowly switched to N_2 atmosphere, and the temperature was increased to 170 ºC. Once the desired temperature was achieved, 2 mL of cesium oleate precursor preheated at 170 ºC was injected swiftly into the solution resulting in yellowish-green solution that led to the formation of $CsPbBr_3$ nanocrystals. After 5 seconds, the solution was placed into an ice-water bath to stop further growth of the nanocrystals. Later, the crude solution was centrifuged at 4500 rpm for 10 min at 15 ºC, the supernatant was discarded, and 1.5 mL of toluene was added to the precipitate and centrifuged again. The as-prepared precipitate was dissolved in toluene with a concentration of 25 mg/mL for further use.

The design and synthesis of the SAMs are reported elsewhere.[18]

Device fabrication

Indium-doped Tin Oxide coated glass substrates (15 mm x 15 mm) with the sheet resistivity of 15 Ω/m^2, purchased from Xinyan Technology Limited were used for the substrate. They were cleaned with the help of ultrasonicator in the mixture of alkaline cleaning concentrate Hellmanex followed by DI water, acetone, and two times from isopropanol (IPA) in a sequence of 10 min each step. Subsequently, the ITOs were transferred to UV/ozone equipment for Ozone treatment of the substrates for 30 min before deposition of hole transport layer. PTAA, purchased from Sigma-Aldrich was dissolved in toluene (2 mg/mL) and deposited on the substrates at 5000 rpm for 30 seconds followed by annealing at 100 ºC for 10 minutes achieving the smooth layer of 10 nm. **EADR03** and **EADR04** were dissolved in isopropanol anhydrous (1 mg/mL). ITO substrates were immersed completely in the SAM solution and kept undisturbed for 4 h at 40 ºC. After that, the substrates were rinsed with IPA for the removal of unattached molecules and

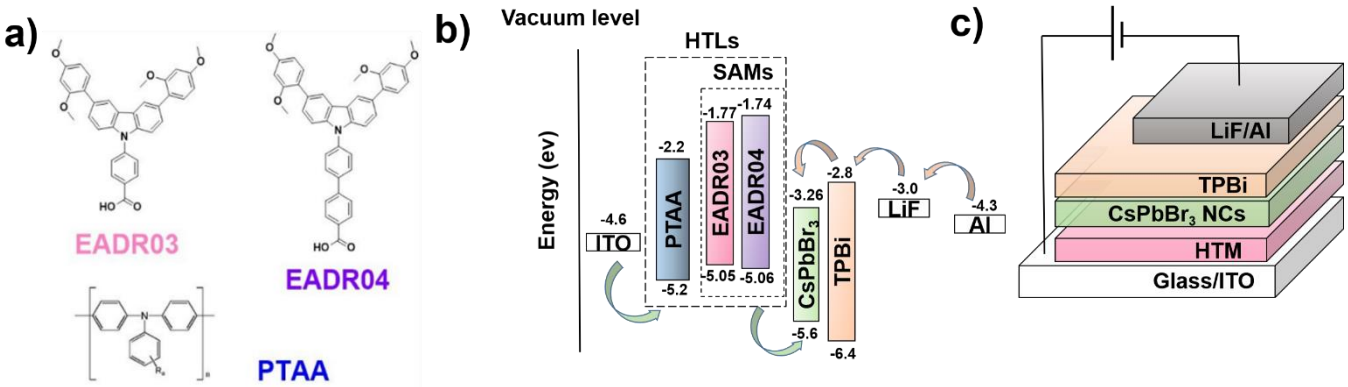

Scheme 1. (a) Schematic representation of the molecular structures of the materials used as HTM in this work; (b) energy levels and (c) device structure of the PeLEDs prepared in this work.

dried with nitrogen. The substrates were transferred to N_2 filled glove box for the further deposition. 50 µL of the QD solution was spin coated on each device at 5000 rpm for 60 s followed by thermal annealing for 20 min at 100 °C. The devices were transferred carefully to the thermal evaporator for the thermal deposition of further layers at the base pressure of $1x10^{-6}$ mbar. 50 nm thin layer of an electron transporting material TPBi {2,2',2''-(1,3,5-Benzinetriyl) -tris(1-phenyl-1-H-benzimidazole)}, 1 nm of Lithium fluoride (LiF) as a buffer layer and 100 nm of aluminum (Al) as cathode was evaporated completing the fabrication process of the PeLEDs forming an active area of 9 mm^2.

Characterization of the Nanocrystals

UV-Vis absorption spectra were measured in a SHIMADZU UV-2401PC spectrophotometer with a 10 mm path length of quartz cuvettes, using toluene as a reference. The fluorescence spectra were carried out in the range of 450-650 nm using a Spectrofluorimeter Fluorolog from Horiba Jobin Yvon Ltd with PMT and InGaAs detectors. The photoluminescence quantum yield (PLQY) was estimated using an ethanolic solution of Coumarine 153 as reference. Three different excitation wavelengths were chosen between the absorbance maximum of the two samples, 435, 445 and 455 nm. In the three cases, the MHP NCs and the Coumarine 153 reference displayed the maximum at 518 and 522 nm, respectively. The calculation of the PLQY was done following equation 1:

$$QY = QY_{ref}\left(\frac{I_{em\,sample}}{I_{em\,ref}}\right)\cdot\left(\frac{Abs_{ref}}{Abs_{sample}}\right) \qquad \text{Equation 1}$$

where QY_{ref} is the quantum yield of the reference, which is 0.544, I_{em} is the emission intensity and Abs the absorbance. The estimation of the PLQY of the NCs did not vary much with the varying excitation wavelength and was thus calculated as 27%, 27.6% and 29.5% for 435 nm, 445 nm and 455 nm excitation wavelengths respectively. The fluorescence spectra of the films were done on samples made of ITO/HTM/MHP NCs/PMMA where PMMA is a thin layer of poly methyl methacrylate (PMMA) deposited on top to prevent degradation.

Time correlated single photon counting (TCSPC) measurements were done on the instrument Edinburgh Instruments LifeSpec-II with an excitation source of 470 nm. The measurements were done at a constant 50 ns for the NCs and 120 ns for the ITO/HTMs/NCs films. The fluorescence decay lifetime was fitted using a bi-exponential function (Equation 2).

$$\tau(t) = A_1 e^{-\left(\frac{t}{\tau 1}\right)} + A_2 e^{-\left(\frac{t}{\tau 2}\right)} \qquad \text{Equation 2}$$

where A_1 and A_2 are the amplitude of the radiative decay lifetime and τ represent the lifetime values. The average lifetime values were estimated using Equation 3:

$$\tau_{average} = \sum \alpha_i \tau_i; \text{ where } \alpha_i = \frac{A_i \tau_i}{\sum A_i \tau_i} \qquad \text{Equation 3}$$

Transmission electron microscopy (TEM) analysis was carried out on a JEOL 1011 microscope.

Atomic Force Microscopy (AFM) measurements were done in tapping mode on a Molecular Imaging model Pico SPM II (pico+) in air conditions using the tip with curvature radius of 1 nm. Images were analyzed using the software Gwyddion 2.62.

Cyclic voltammetry was performed using a computer controlled potentiostat in a three-electrode cell. The reference electrode was an Ag/AgCl electrode, the working electrode was made of glassy carbon and a platinum wire was used as counter-electrode. The measurements were done in an electrolyte solution in toluene containing 0.1 M $TBAPF_6$ and ferrocene as internal reference.

Characterization of the devices

The variations of the luminance and the current density as a function of the applied bias were recorded using a Konica Minolta IS 100 camera and a Keithley 2400 Unit as voltage/current source, respectively. The lifetimes of the diodes were measured by applying a constant current of 2 mA to the devices and monitoring the luminance with the time until it reached values of 1 cd/m^2. The electroluminescence of the devices was recorded with the help of a fiber connected to a USB4000 spectrometer from Ocean Optics and applying a constant voltage of 9 V.

Results and discussion

$CsPbBr_3$ NCs were synthesized following the method reported by Protesescu at al.[24] TEM analysis evidence the formation of nearly cube shaped NCs with average size of 7.6 ± 1.9 nm (see Fig. S1a and Fig. S1b). The XRD pattern (Fig. S1c) reveal peaks located at 13.7º, 15.1º, 21.3º, 24.1º, 30.1º, 33.8º, 37.5º and 45.9º that correspond to the reflections of the crystal planes (100), (110), (200), (211) and (202) corresponding to the cubic structure. Optical properties, investigated by UV-Visible absorption and photoluminescence (PL) measurements (Fig. S2) were recorded from the colloidal dispersion of NCs. The PL maximum after excitation at 424 nm was located at 518 nm with a full width at half maximum (FWHM) of 23 nm while the PL quantum yield (PLQY), estimated using Coumarine 153 as reference, gave a value of 29.5%. The band gap has been estimated in 2.34 eV (Fig. S3) whereas the valence band has been calculated by cyclic voltammetry to be at -5.6 eV (Fig. S1d). Combining both measurements, the conducting band (CB) has been estimated to be at -3.26 eV. These values agree with those reported previously in the literature calculated by cyclic

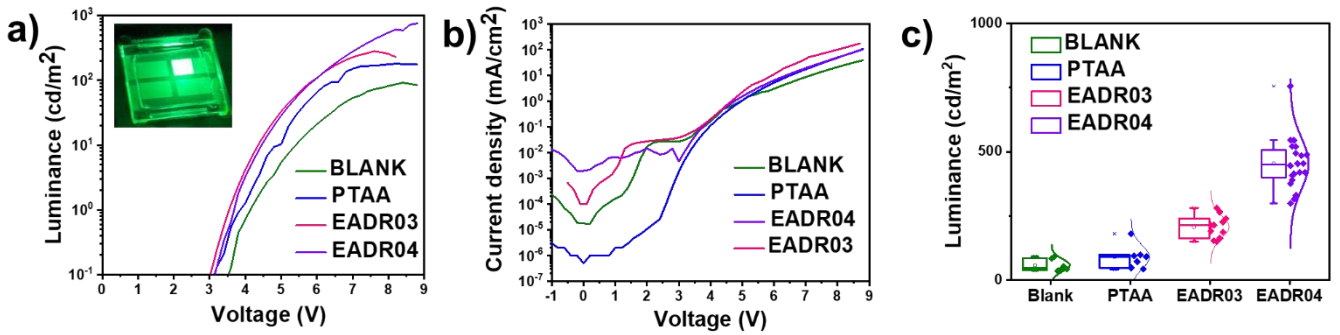

Fig. 1. Performance of the PeLEDs prepared with different HTMs: a) Variation of the luminance as a function of the applied bias, b) evolution of the current density with the applied bias; and c) device performance statistics of the luminance values achieved on over 30 devices containing blank, PTAA, **EADR03** and **EADR04**.

voltammetry and UPS.[25,26,27] Finally, the average lifetime of the fluorescence decay of the nanocrystals is 5.7 ns (Fig. S4).

The MHP NCs were deposited onto the HTMs in a sandwich structure (see Scheme 1b and 1c) made of ITO/SAMs (< 5 nm) or PTAA (10 nm)/$CsPbBr_3$/TPBi (50 nm)/LiF (1nm)/Al (100 nm). In this structure, the SAMs and PTAA act as hole injection materials, the $CsPbBr_3$ as emissive layer, TPBi as an electron transport material, LiF as a cathode buffer material and Al as an electrode. The reference device, named as Blank, was prepared without the hole transport material following the structure ITO/$CsPbBr_3$/TPBi/LiF/Al. The energy levels of the HTMs, TPBi and LiF (Scheme 1b) were taken from the literature.[28,18] The performance of the devices was evaluated by applying an external bias and recording the variation of the luminance and current density (Fig. 1a and 1b). All the devices emit light under the application of an external bias, although the maximum luminance achieved differs depending on the HTM (Table 1). The best results are obtained with the SAM **EADR04**, followed by **EADR03** and then the references with PTAA and without HTM. Fig. 1c shows all the measured luminance of different set of devices demonstrating the consistency of the observed values, whereas Figure S5 show the current efficiency variation with the applied bias. Regarding the turn-on voltage, the devices prepared with SAMs show the lowest values while the blank display the highest voltage. On the one hand, the HOMO energy levels of the SAMs can effectively inject holes into the valence band (VB) of the MHP NCs having intermediate values within the work function of the ITO and the VB of the MHP NCs, in comparison to PTAA. On the other hand, the LUMO level is higher in **EADR03** and **EADR04** than in PTAA suggesting that they will act as better electron blocking layers confining the charges in the emissive layer and promoting radiative recombination. In order to have a better understanding of the performance of the devices, we carried out morphological and optical characterization of the emissive layer deposited onto the HTM.

Table 1. Performance of PeLEDs prepared with different HTMs.

HTMs	Maximum luminance (cd/m^2) [Average values]	Turn-on Voltage[a] V_{on} (V)	Lifetime[b] T_{50}/T_t (s)
Blank	92 [57.5 ± 24.4]	4	4/354
PTAA	180 [89.1 ±45.9]	3.2	6/596
EADR03	281 [207.2 ±43.8]	3.1	4/384
EADR04	756 [453.6 ± 101.2]	3.1	11/1157

[a] Turn-on voltage of the devices is the voltage at which devices achieve 0.1cd/m^2 of luminance.

[b] The lifetime of the devices: T_{50} time range in which luminance decrease to half of its initial value under a constant applied current of 2 mA, T_t is defined as the time range at which the luminance of the devices is higher than 1 cd/m^2 under a constant applied current of 2 mA.

The surface topography was analysed by AFM (Fig. 2), whose images show the coverage of the HTM by the MHP NCs. The average roughness RMS values, Table 2, indicate small differences between the samples lower than 1 nm being the film on top of the ITO the rougher, whereas both films on the SAMs are the smoothest. Considering that the mean average size of the NCs is 7.6 nm, the RMS values close to 5 nm suggest that the film formation is not completely homogenous. Yet, the absence of shortcuts and the comparison of the light emission and turn on voltage values between the devices without HTM (the blank) and those with **EADR03** and **EADR04** indicate that such heterogeneities have a negligible effect on the light emission in the devices. In addition, we have analysed the images to get more information. The estimated grain density reveal that the blank contains more NCs than the other samples in the same area which will account for the differences in the RMS. The estimation of the volume, defined as the total volume between the grain surface and the plane, reveal that for the blank and the PTAA sample this is higher than for **EADR03** and **EADR04**. Therefore, despite the similar RMS values and grain density, the layer of MHP NCs deposited on top of PTAA is thicker than onto **EADR03** and **EADR04**. Height threshold image analysis, shown in Figure S6, support this observation and suggest that the MHP NCs are deposited as a multilayer onto

the ITO, as a bilayer onto the SAMs whereas for PTAA the NCs film shows intermediate values between two and three layers. Therefore, the presence of SAMs influences the deposition of the MHP NCs.

Table 2. Characterization of the MHP NCs deposited on top of different HTMs/ITO samples: value of the water contact angle, roughness mean average (RMS), grain density and volume between the grain surface and the plane, estimated from AFM measurements

ITO/HTMs/NCs	Contact angle (º)[a]	RMS (nm)	Grain density (grains·μm^{-2})	Volume (μm^3)
Blank	8.13	5.04	4218	0.069
PTAA	88.15	4.67	3353	0.026
EADR03	50.19	4.13	3494	0.017
EADR04	51.63	4.38	3343	0.019

[a] values taken from ref [18]

The wettability of the HTM/ITO substrates can be inferred by the measurement of the value of the contact angle formed by water droplets. The results, taken from the literature and shown in Table 2, indicate that the nature of the substrate can be tuned from hydrophilic character in the case of the bare ITO, to hydrophobic when PTAA is deposited. Despite these differences, the NCs were deposited by spin coating forming a continuous film.

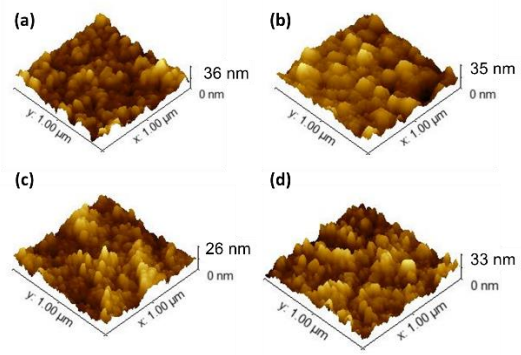

Fig. 2. AFM images of the films of ITO/HTM/$CsPbBr_3$ NCs where HTM was: (a) blank, (b) PTAA, (c) **EADR03**, and (d) **EADR04**.

Optical characterization of the films of ITO/HTMs/MHP NCs/PMMA has also been performed and the results are shown in Figure S7. The UV-Visible absorption spectra display clear excitonic peaks with a maximum at 475 nm for the NCs deposited on SAMs, which agree with the value observed in the solution of the NCs. Photoluminescence (PL) spectra are characterized by a single peak assigned to the NCs, which is located at 513 nm in the **EADR03** and **EADR04** samples, respectively, and at 517 nm for both PTAA and the blank. The measurement of the FWHM (Table 3) indicate that the PL peaks corresponding to **EADR03** and **EADR04** are slightly broader than those of PTAA and the Blank, that are coincident with the measurement of the NCs in solution. The broadening of the signal is assigned to the increased dispersion of NCs size when the MHP NCs are in contact with the SAM molecules. The methoxy substituents can interact with the Pb atoms and Cs^+ in the surface by donating electrons through a Lewis acid-base reaction,[29] which induces the 4 nm-shift towards the blue of the PL peak. In order to have more information, we have compared the PL of the MHP NCs in solution with that of the solutions of NCs mixed with PTAA or with **EADR04**. The result, shown in Figure S8, show similar behaviour in the PL maximum, pointing to an effective interaction of the functional groups of the SAM with the surface of the NCs that take place in seconds. This observation is coincident with the effect, observed by AFM analysis, that the presence of SAMs has on film formation.

Time correlated single photon counting (TCSPC) measurements were also performed. The fluorescence emission kinetics indicate that the signal decays faster in the presence of **EADR04** (see Table 3) but is much slower than that of the NCs in solution. The shorter average decay time observed in the samples with **EADR04** could be assigned to more efficient extraction of the carriers by the SAMs than by PTAA or to the formation of defects at the interface between the SAMs and the MHP NCs that could act as charge traps. However, the performance of the complete devices (shown in Fig. 1), suggest that the former hypothesis is more plausible than the later and that **EADR04** acts as efficient selective contact for the charge carriers, better than PTAA. In this regard, the observation of two decay lifetimes is assigned to the radiative recombination due to surface defects (fast decay) and into the bulk (slow decay). Interestingly, the addition of the **EADR04** SAMs decreases the lifetime and weighting coefficient for the processes arising at the surface whereas the relative proportion of processes taking place in the bulk increases. It is noteworthy that, despite having the same peripheral substituents, **EADR04** show shorter PL lifetime than **EADR03**, pointing to the fact that the effect of the SAMs goes beyond the potential interaction with the surface of the NCs and is related as well to the charge transport ability of the molecules.

Table 3. Fluorescence characterization of the MHP NCs deposited on top of different HTMs/ITO samples: maximum intensity wavelength and FWHM of the peak estimated from steady state fluorescence, and average fluorescence lifetime decays (τ_{av}), lifetime values (τ) and weighting coefficients for each decay channel (A).

ITO/HTMs/NCs	λ_{max} (nm)	FWHM (nm)	τ_{av} (ns)	τ_1 (ns)	A_1 (%)	τ_2 (ns)	A_2 (%)
Blank	517	18	69.9	17.2±0.7	29.8	92.4±3.1	70.2
PTAA	517	18	71.1	21.1±1.4	33.1	95.7±5.9	66.9
EADR03	513	22	67.1	19.1±1.0	34.5	92.5±6.0	65.5
EADR04	513	27	56.2	15.4±2.9	23.1	68.5±6.1	76.9

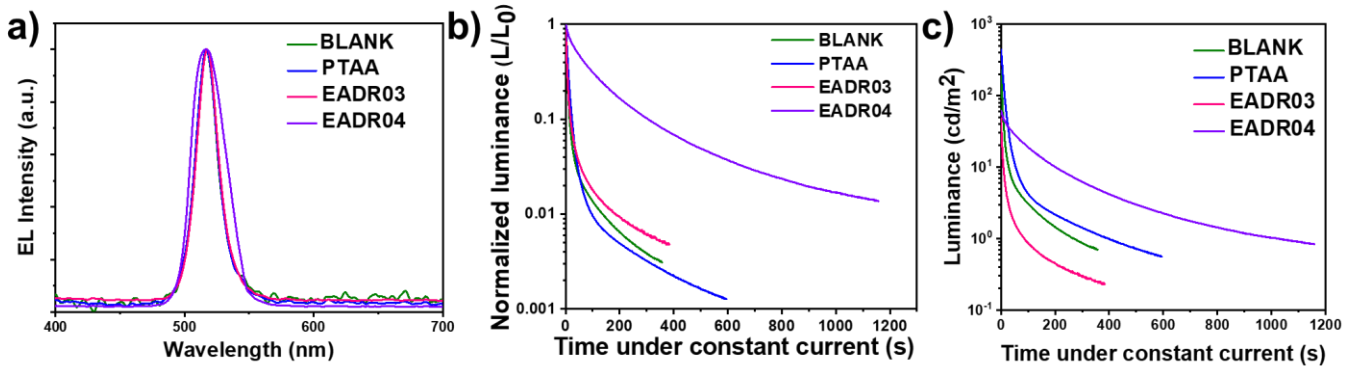

Fig. 3. (a) Electroluminescence measured after applying a constant voltage of 9V to PeLEDs prepared with SAMs as HTM and with PTAA and blank; (b) Normalized luminance vs time to show the operational lifetime of the devices prepared with different HTM while applying a constant current of 2 mA, and (c) operational lifetime recorded under the same conditions displayed using absolute values of luminance.

The electroluminescence (EL) recorded after applying a constant voltage of 9 V to the complete devices is displayed in Fig. 3 where it can be seen that the EL peak intensity for the devices is at 517 nm. The position and width of the EL signal in complete devices is coincident to that obtained by PL measurements in films made of ITO/PTAA/MHP NCs, pointing that the light emission has the same origin for the Blank and the PTAA in both cases independently of the excitation source and that it corresponds to the MHP NCs. For the devices containing **EADR03** and **EADR04**, the EL maximum is at the same position than for the Blank and the PTAA, shifted 4 nm in comparison to their corresponding PL spectra. Therefore, the source of the electroluminescence is similar in all the devices despite the nature of the HTM. Taking into account the results seen by TCSPC where the dominant component corresponds to the processes in the bulk, we therefore, infer that electroluminescence arises mainly from the radiative recombination taking place in the bulk. Thus, although the functional groups of the SAMs interact with the surface of the NCs, inducing a small shift in the PL maximum, they do not influence the origin of the electroluminescence.

Finally, the stability of the devices was also analyzed. For that, a constant current of 2 mA was applied to the devices and the evolution of the emitted light was recorded *versus* time. The device's total lifetime (T_t), defined as the time when the light output from the devices is higher than 1 cd/m^2 and the T_{50}, defined as the time for the brightness to decrease to the half of its initial value, are shown in Table 1. Fig. 3b, normalized luminance decay, and 3c, luminance decay, report the evolution of the light emission intensity with time of the devices prepared with **EADR03**, **EADR04**, PTAA and the blank. An exponential decrease can be seen in all the cases, which is more pronounced in the case of the PTAA. The decay has been assigned in the literature to: (i) the initial migration of mobile ions in the MHP NCs towards the local defects induced by applied electrical field, that can generate a transient increase of light emission intensity, that is not observed in these cases,[12,16,29], and (ii) the unbalanced charge injection leading to charge accumulation at the interface that can promote interfacial degradation.[30] Other factors accounting for the operational instability in PeLEDs are undesired electrochemical reactions at the interface and accumulation of heat due to the Joule effect.[31] Light emission in

EADR04 devices decreases less rapidly and results in the most stable LEDs, with an increase in the stability of more than 50% in comparison to PTAA. Noticeably, light emission from **EADR03** decreases in similar manner to the blank and the PTAA devices, with lifetime values comparable to the blank.

The degradation rate was also investigated by measuring the current density dependence on the applied bias before and after the lifetime measurements. It can be seen from Fig. 4 that the variation of the current density with the applied bias in non-degraded devices show a change in the regime from linear to exponential that can be explained by the space charge limited current (SCLC) model, as it has been observed in hybrid light emitting devices.[32,33] This accounts for the charge accumulation at the interface, which often correspond to electron accumulation due to the better charge transport properties of the HTMs into the photoactive layer. Therefore, the exponential increase of the current density occurs when the balance in charge injection into the photoactive layer is achieved and is related to the value of the turn-on voltage where the apparition of luminance is observed. In our case, the SAM-containing devices need lower voltages to turn on than PTAA devices and the blank, which accounts for the hole injection ability of the SAMs. However, after the lifetime measurements, during which the devices had been exposed to the application of a constant current for a given period of time, the devices prepared with **EADR03**, PTAA or without HTM displayed a resistive behaviour. On the contrary, for **EADR04** we can still observe the same behaviour that non-degraded devices, strongly suggesting that the molecule maintains for a longer period of time its properties adding stability to the device.

Considering the overall performance of the devices and the results of the optical characterization, the degradation is assigned to the unbalanced charge injection caused by interfacial degradation. In this sense, we would like to remark that, as reported before, when **EADR04** is used in perovskite solar cells, the stability increases, which has been assigned to the passivation of the perovskite film and the increased resistance to thermal degradation. **EADR03** has alike anchoring group (-COOH) and terminal moiety (4'- (3,6-bis(2,4-dimethoxyphenyl)- 9*H*-carbazol- 9-y) but different molecular bridge than **EADR04**. In this work, we have observed by PL measurements that the terminal moiety interacts with the surface of the MHP NCs, affecting the formation of the film of MHP NCs, as seen by AFM. Moreover, the application of SAMs decreases the turn on voltage and increases the luminance values. However, from the measurements of stability and degradation, **EADR03** and **EADR04** behave differently, so we have discarded that this interaction is the sole responsible for the better performance of the device. Hence, we explain the

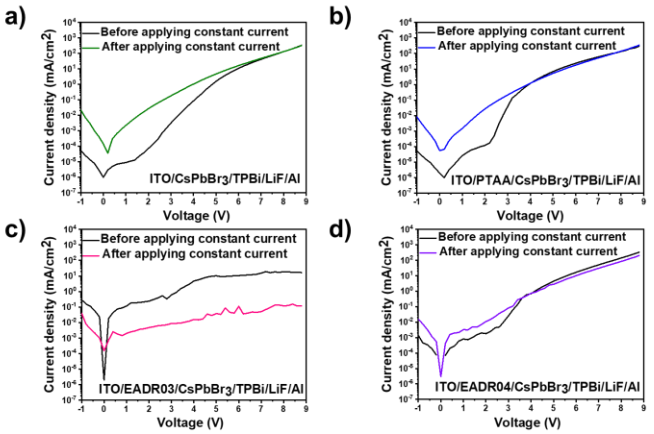

Fig. 4. Current density variation with the application of an external bias in devices before and after the measurement of lifetime stability that consist in the application of 2 mA until the luminance decays below 1 cd/m^2 (see the value of the lifetime T_t in Table 1 for the time of application in each device). The measurements correspond to devices made with: (a) no HTM, (b) PTAA, (c) **EADR03**, and (d) **EADR04**.

extended lifetime of the MHP NCs LEDs mainly because of (i) the better endurance of the SAMs **EADR04** to the decomposition induced by operando conditions (heat generation caused by Joule effect) and (ii) because of the improved charge balance into the device that avoids charge accumulation at the interface. The addition of the second benzyl moiety in the linker section of the **EADR04** molecule improves electron delocalization in the molecule, which in turn increases its electronic and thermal stability.[34,35]

Conclusions

From our experiments we conclude that the PeLEDs made with the carbazole-based SAM molecules **EADR04** show better performance than the reference devices (the one with PTAA as hole transport material and the blank prepared without any HTM). The investigation demonstrates that, first, the use of both **EADR03** and **EADR04** SAMs, influence the formation of the films made by the NCs and increase the luminance of the PeLEDs whereas lowering the turn-on voltage due to the enhanced charge injection ability of the SAMs in comparison to PTAA. And second, that the fine tuning of the SAM structure, such as the addition of a second phenyl moiety in the linkage part of the **EADR04**, enhance the operational stability of the devices due to the increased resistance of the SAM to decomposition induced by operando conditions.

The low consumption of materials required for the device preparation, their low cost and beneficial influence on the performance make such SAMs promising materials for the further development of perovskite LED.

Author Contributions

SK and JGS prepared and characterized the devices with the help of EMF, MI and SK prepared the MHP NCs under the guidance of LM, EA and DAG designed and synthesised the carbazole derivatives **EADR03**

and **EADR04** with the help of EP. SK, EMF and EP analysed the results. All the authors contributed to the manuscript preparation and revision.

Conflicts of interest

There are no conflicts to declare.

Acknowledgements

S.K. acknowledges the program "Vicente López" from EURECAT for financial support. Funding from MINECO (project PID2019-109389RB-I00) and SGR-AGAUR (project 2017SGR00978) is also acknowledged. E.P. is also thankful to ICIQ, CERCA, and ICREA for financial support. D.A.G. acknowledges financial support from MINECO predoctoral fellowship (BES-2017-082439).

Notes and references

1 H. Cho, Y. H. Kim, C. Wolf, H. D. Lee and T. W. Lee, *Adv. Mater.*, 2018, **30**, 1–24.

2 A. Kojima, K. Teshima, Y. Shirai and T. Miyasaka, *J. Am. Chem. Soc.*, 2009, **131**, 6050–6051.

3 J. Y. Kim, J. W. Lee, H. S. Jung, H. Shin and N. G. Park, *Chem. Rev.*, 2020, **120**, 7867–7918.

4 A. Liang, K. Wang, Y. Gao, B. P. Finkenauer, C. Zhu, L. Jin, L. Huang and L. Dou, *Angew. Chemie - Int. Ed.*, 2021, **60**, 8337–8343.

5 J. Miao and F. Zhang, *J. Mater. Chem. C*, 2019, **7**, 1741–1791.

6 C. Li, H. Wang, F. Wang, T. Li, M. Xu, H. Wang, Z. Wang, X. Zhan, W. Hu and L. Shen, *Light Sci. Appl.*, 2020, **9**, 31.

7 Q. Zhang, Q. Shang, R. Su, T. T. H. Do and Q. Xiong, *Nano Lett.*, 2021, **21**, 1903–1914.

8 Q. A. Akkerman, G. Rainò, M. V. Kovalenko and L. Manna, *Nat. Mater.*, 2018, **17**, 394–405.

9 Z. K. Tan, R. S. Moghaddam, M. L. Lai, P. Docampo, R. Higler, F. Deschler, M. Price, A. Sadhanala, L. M. Pazos, D. Credgington, F. Hanusch, T. Bein, H. J. Snaith and R. H. Friend, *Nat. Nanotechnol.*, 2014, **9**, 687–692.

10 Y. H. Kim, S. Kim, A. Kakekhani, J. Park, J. Park, Y. H. Lee, H. Xu, S. Nagane, R. B. Wexler, D. H. Kim, S. H. Jo, L. Martínez-Sarti, P. Tan, A. Sadhanala, G. S. Park, Y. W. Kim, B. Hu, H. J. Bolink, S. Yoo, R. H. Friend, A. M. Rappe and T. W. Lee, *Nat. Photonics*, 2021, **15**, 148–155.

11 H. Moon and H. Chae, *Adv. Opt. Mater.*, 2020, **8**, 1–5.

12 F. Ye, Q. Shan, H. Zeng and W. C. H. Choy, *ACS Energy Lett.*, 2021, **6**, 3114–3131.

13 J. Li, H. L. Cao, W. Bin Jiao, Q. Wang, M. Wei, I. Cantone, J. Lü and A. Abate, *Nat. Commun.*, 2020, **11**, 310.

14 A. Filippetti, S. Kahmann, C. Caddeo, A. Mattoni, M. Saba, A. Bosin and M. A. Loi, *J. Mater. Chem. A*, 2021, **9**, 11812–11826.

15 B. Zhang, L. Goldoni, C. Lambruschini, L. Moni, M. Imran, A. Pianetti, V. Pinchetti, S. Brovelli, L. De Trizio and L. Manna, *Nano Lett.*, 2020, **20**, 8847–8853.

16 L. Xu, J. Li, B. Cai, J. Song, F. Zhang, T. Fang and H. Zeng, *Nat. Commun.*, 2020, **11**, 3902.

17 E. Yalcin, M. Can, C. Rodriguez-Seco, E. Aktas, R. Pudi, W. Cambarau, S. Demic and E. Palomares, *Energy Environ. Sci.*, 2019, **12**, 230–237.

18 E. Aktas, N. Phung, H. Köbler, D. A. González, M. Méndez, I. Kafedjiska, S. H. Turren-Cruz, R. Wenisch, I. Lauermann, A. Abate and E. Palomares, *Energy Environ. Sci.*, 2021, **14**, 3976–3985.

19 L. Li, Y. Wu, E. Li, C. Shen, H. Zhang, X. Xu, G. Wu, M. Cai and W.-H. Zhu, *Chem. Commun.*, 2019, **55**, 13239–13242.

20 A. Al-Ashouri, A. Magomedov, M. Roß, M. Jošt, M. Talaikis, G. Chistiakova, T. Bertram, J. A. Márquez, E. Köhnen, E. Kasparavičius, S. Levcenco, L. Gil-Escrig, C. J. Hages, R. Schlatmann, B. Rech, T. Malinauskas, T. Unold, C. A. Kaufmann, L. Korte, G. Niaura, V. Getautis and S. Albrecht, *Energy Environ. Sci.*, 2019, **12**, 3356–3369.

21 F. Huang, H. Liu, X. Li and S. Wang, *Nano Energy*, 2020, **78**, 105399.

22 Q. Huang, J. Cui, H. Yan, J. G. C. Veinot and T. J. Marks, *Appl. Phys. Lett.*, 2002, **81**, 3528–3530.

23 A. Rana, A. Kumar, S. Chand and R. K. Singh, *J. Appl. Phys.*, 2019, **125**, 053102.

24 L. Protesescu, S. Yakunin, M. I. Bodnarchuk, F. Krieg, R. Caputo, C. H. Hendon, R. X. Yang, A. Walsh and M. V. Kovalenko, *Nano Lett.*, 2015, **15**, 3692–3696.

25 W. Chen, X. Tang, P. Wangyang, Z. Yao, D. Zhou, F. Chen, S. Li, H. Lin, F. Zeng, D. Wu, K. Sun, M. Li, Y. Huang, W. Hu, Z. Zang and J. Du, *Adv. Opt. Mater.*, 2018, **6**, 1–7.

26 V. K. Ravi, G. B. Markad and A. Nag, *ACS Energy Lett.*, 2016, **1**, 665–671.

27 S. Pradhan, D. Bhujel, B. Gurung, D. Sharma, S. Basel, S. Rasaily, S. Thapa, S. Borthakur, W. L. Ling, L. Saikia, P. Reiss, A. Pariyar and S. Tamang, *Nanoscale Adv.*, 2021, **3**, 1464–1472.

28 Y. Lu, Z. Wang, J. Chen, Y. Peng, X. Tang, Z. Liang, F. Qi and W. Chen, *J. Lumin.*, 2021, **234**, 117952.

29 S. Lee, D. Bin Kim, J. C. Yu, C. H. Jang, J. H. Park, B. R. Lee and M. H. Song, *Adv. Mater.*, 2019, **31**, 1–17.

30 T. Fang, T. Wang, X. Li, Y. Dong, S. Bai and J. Song, *Sci. Bull.*, 2021, **66**, 36–43.

31 Q. Dong, L. Lei, J. Mendes and F. So, *J Phys Mater.*, 2020, **3**, 012002.

32 L. Xu, G. Liu, H. Xiang, R. Wang, Q. Shan, S. Yuan, B. Cai, Z. Li, W. Li, S. Zhang and H. Zeng, *Appl. Phys. Rev.*, 2022, **9**, 021308.

33 L. P. Lu, D. Kabra and R. H. Friend, *Adv. Funct. Mater.*, 2012, **22**, 4165–4171.

34 Z. Li, F. Wu, H. Lv, D. Yang, Z. Chen, X. Zhao and X. Yang, *Adv. Mater.*, 2015, **27**, 6999–7003.

35 R. Báez-Grez and R. Pino-Rios, *ACS Omega*, 2022, **7**, 21939–21945.